Controllable synthesis of triangle taper-like cobalt hydroxide and cobalt oxide†

Chaohe Xu, Jing Sun* and Lian Gao*

Received 16th June 2010, Accepted 8th October 2010
DOI: 10.1039/c0ce00311e

Triangle taper-like β-$Co(OH)_2$ and mesoporous Co_3O_4 microcrystals are synthesized by a simple solid-state crystal reconstruction approach. Ostwald ripening and successive dissolve-reconstruction processes were used to explain the formation mechanism. The electrochemical properties of the β-$Co(OH)_2$ and mesoporous Co_3O_4 electrodes were investigated by cyclic voltammetry measurements. The specific capacitances are 137.6, 124.8, 108.8 and 98.0 F g^{-1} at scan rates of 5, 10, 20 and 50 mV s^{-1} for β-$Co(OH)_2$; 91.5, 97.4, 90.7 and 70.9 F g^{-1} for Co_3O_4 sample at scan rates of 5, 10, 20 and 50 mV s^{-1}. The magnetic properties also have been investigated at room temperature.

Introduction

Nanostructure materials are of great importance in many applications due to their special properties;[1,2] in particular, they have attracted intensive research efforts in catalysts,[3] delivery of drugs,[4] lithium ion batteries (LIBs),[5] and electrochemical supercapacitors.[6] Many cobalt-based nanostructures, such as cubes,[7,8] wires,[9] rods[10] and hierarchical columns[11] have been synthesized by various methods. For example, virus-templated Co_3O_4 nanowires have been demonstrated as improved anode materials for LIBs.[12] Lou and coworkers prepared needle-like Co_3O_4 nanotubes which showed ultrahigh capacity and rate capability.[13] Shen and coworkers synthesized Co_3O_4 nanorods by the calcinations of cobalt hydroxide carbonate precursor, which showed superior catalytic properties at 77 K.[14]

Since mesoporous structures can provide large BET surface areas and channels for ion diffusion, they have received intensive attention for electrochemical applications. Single-crystal Co_3O_4 of porous structures templated by mesoporous silica have been prepared.[15–17] Mesoporous Co_3O_4 nanowire arrays which were synthesized *via* a facile template-free and ammonia evaporation-induced method, exhibited an excellent electrochemical performance for LIB electrode materials.[18,19] Lou and coworkers reported the solid formation of mesoporous Co_3O_4 nano-needles with a 3D single-crystalline framework, which demonstrated ultrahigh lithium storage properties.[20] Zhan and coworkers have prepared mesoporous Co_3O_4 with a hexagonal sheet-like structure by a simple solid-state formation process.[21] Therefore, the solid-state formation process was widely adopted for the preparation of cobalt oxide.

Recently, mesoporous structures of $Co(OH)_2$ and Co_3O_4 have been synthesized as electrode materials for supercapacitors. For example, Xiong *et al.* and Wang *et al.* developed a morphologically tunable way[22] and applied Co_3O_4 nanorods[23] as electrode materials for supercapacitors. Zhou and coworkers also prepared mesoporous $Co(OH)_2$ films on different substrates for supercapacitors.[24] In addition, composites such as TiO_2/$Co(OH)_2$,[25] RuO_2/Co_3O_4[26] and Co_3O_4/carbon nanotubes[27] have been synthesized as electrode materials for supercapacitors. Although a lot of reports have been published on $Co(OH)_2$ and Co_3O_4 nanostructures and their application as the electrode materials for energy storage devices. However, to the best of our knowledge, there are no reports on the synthesis of triangle taper-like β-$Co(OH)_2$ and mesoporous Co_3O_4 microcrystal.

In the present paper, we report the synthesis of triangle taper-like β-$Co(OH)_2$ and mesoporous Co_3O_4 microcrystals *via* a simple solid-state crystal reconstruction approach. Their electrochemical performance as electrode materials for supercapacitors and magnetic properties has been investigated in this study.

Experimental

All chemicals were of analytical grade and used as received. $Co(OH)_2$ and Co_3O_4 samples were prepared as follows. Typically, 50 mL deionized water and 50 mL ammonia solution (25–28%) were added into a 250 mL three-necked flask, which was immersed into an oil bath at 95–100 °C. Then, 10 mL of 0.1 M $Co(NO_3)_2 \cdot 6H_2O$ was added dropwise. The reactants were magnetically stirred for 120 min and cooled down to room temperature. The product was harvested by filtration and washed with distilled water and absolute ethanol for several times and dried at 60 °C overnight. The pink powder was calcined at 400 °C for 4 h to get Co_3O_4.

Phase identification was performed on the powder X-ray diffraction pattern (XRD), using D/max 2550V X-ray diffraction-meter with Cu-Kα irradiation at $\lambda = 1.5406$ Å. Field-emission scanning electron microscopy (FESEM), transmission electron microscopy (TEM) and high resolution transmission electron microscopy (HRTEM) were performed on JEM-2100F electron microscope with an accelerating voltage of 200 kV. The specific surface area was investigated by Brunauer-Emmett-Teller (BET) method at 77 K in N_2 atmosphere using Micromeritics ASAP 2010 surface area analyzer.

The State Key Lab of High Performance Ceramics and Superfine Microstructure, Shanghai Institute of Ceramics, Chinese Academy of Sciences, 1295 Ding Xi Road, Shanghai, 200050, China. E-mail: jingsun@mail.sic.ac.cn; Fax: +86 21 52413122; Tel: +86 21 52412718; liangao@mail.sic.ac.cn

† Electronic supplementary information (ESI) available: Additional XRD curves. See DOI: 10.1039/c0ce00311e

All the electrochemical experiments were carried out by cyclic voltammetry (CV) in a three-electrode cell system using Parstat 2273 electrochemical station (Princeton applied research Co., Ltd., USA). The electrodes was prepared by the following steps. The mixture containing 80 wt% active materials, 10 wt% acetylene black and 10 wt% polyvinylidene fluoride (PVDF) binder were mixed well, and then pressed onto nickel foam (10 MPa) that served as a current collector (surface is 1 cm^2). The typical mass load of electrode material is 5–8 mg. The electrolyte was 2 M KOH solution for $Co(OH)_2$ and Co_3O_4. The electrochemical behavior was characterized within a potential window of −0.3 to 0.5 V *vs.* SCE for $Co(OH)_2$ and −0.2 to 0.5 V *vs.* SCE for Co_3O_4. Platinum wire was used as a counter electrode. Magnetization was measured by a commercial Physical Properties Measurement System (PPMS, Quantum Design Inc.) under 2 T magnetic field at room temperature.

Results and discussion

1. Characterization of cobalt hydroxide and cobalt oxide structures

Fig. 1a shows the XRD pattern of the as-prepared triangle taper-like $Co(OH)_2$. All the diffraction peaks are well indexed to pure hexagonal phase of β-$Co(OH)_2$ according to JCPDS 30-0443 (hexagonal phase, space group: $P\bar{3}m1$, a_0 = 3.183 Å, c_0 = 4.652 Å). Fig. 2a and c show the TEM and SEM images of the obtained β-$Co(OH)_2$, from which it is obviously observed that most of the products are triangle taper-like microcrystals with diameters ranging from sub-100 nm to 1μm and lengths from 2.5–3.5 μm. The β-$Co(OH)_2$ microcrystals grew along [001] direction with *d*-spacing as 0.46 nm are well crystallized from the HRTEM image and SAED patterns (inset in Fig. 2a). The XRD pattern of the products obtained by annealing β-$Co(OH)_2$ at 400 °C for 4 h is shown in Fig. 1b. All the diffraction peaks are well indexed to pure cubic phase of Co_3O_4 according to JCPDS 42-1467 (cubic phase, space group: $Fd3m$, a_0 = 8.084 Å), indicating the formation of Co_3O_4 after annealing. The acute diffraction peaks verify good crystallization of the Co_3O_4 sample. They kept the triangle taper-like shape as shown in Fig. 2b. The porous structures could clearly be observed both in the low (Fig. 2b) and HRTEM image (Fig. 3b). The mesoscale pores formed in the transferring process of β-$Co(OH)_2$ to Co_3O_4 and phase transformation occurred at the same time (from hexagonal β-$Co(OH)_2$ to cubic phase Co_3O_4). As we known, β-$Co(OH)_2$ has a brucite-like layered structure and Co_3O_4 has a cubic structure.[13] During the transformation process, Co^{3+} diffuse into the interlayer space and half of the Co^{2+} in the brucite-like sheets are also oxidized into Co^{3+} [13]. The cubic Co_3O_4 microcrystals grew along the [111] direction and the *d*-spacing is 0.46 nm, indicating that the (001) plane of β-$Co(OH)_2$ changed to (111) plane of Co_3O_4 directly.[13] Similar results are observed in the previous reports which the same *d*-spacing value of $Co(OH)_2$ and Co_3O_4 are obtained.[11,13] The inset in Fig. 2b is the corresponding SAED patterns, indexing as (111), (2–20) and (3–11) planes which belong to cubic Co_3O_4 phase. The pore diameters are about 5–10 nm as shown in the HRTEM image.

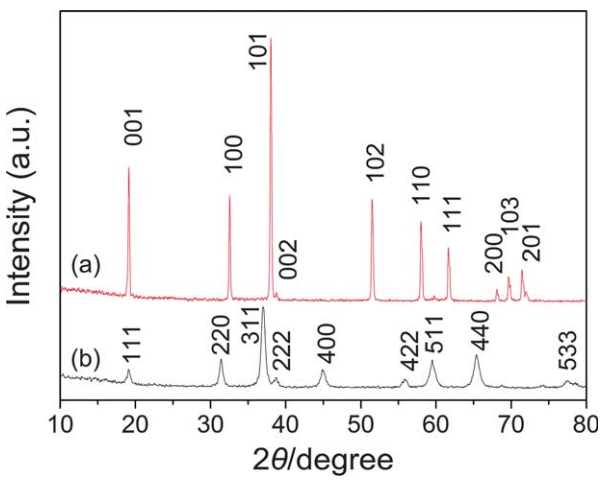

Fig. 1 XRD patterns of the triangle taper-like samples (a) β-$Co(OH)_2$, (b) Co_3O_4.

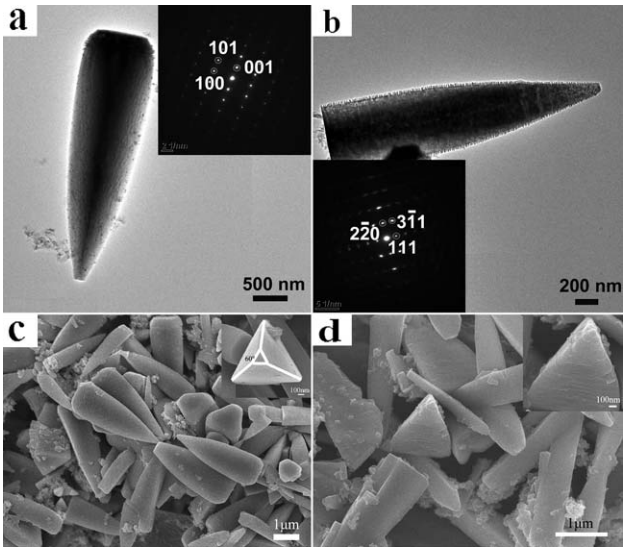

Fig. 2 TEM images of the triangle taper-like samples (a) β-$Co(OH)_2$, (b) Co_3O_4; SEM images of the triangle taper-like samples (c) β-$Co(OH)_2$, (d) Co_3O_4.

Fig. 4 shows the N_2 adsorption/desorption isotherms at 77 K of $Co(OH)_2$ and Co_3O_4 samples and the pore size distribution curves of the samples. For $Co(OH)_2$, the BET surface areas are 228 $m^2\ g^{-1}$ with an average pore size of 2.6 nm. The BET surface area is 47 $m^2\ g^{-1}$ for Co_3O_4 mesostructures and the pore size is 4–20 nm from the bimodal curves. The average pore diameter is

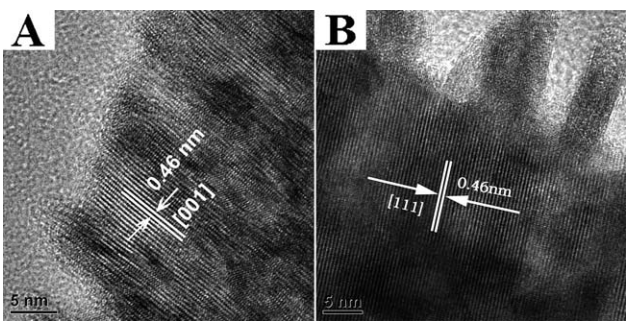

Fig. 3 HRTEM images of samples (a) β-$Co(OH)_2$, (b) Co_3O_4.

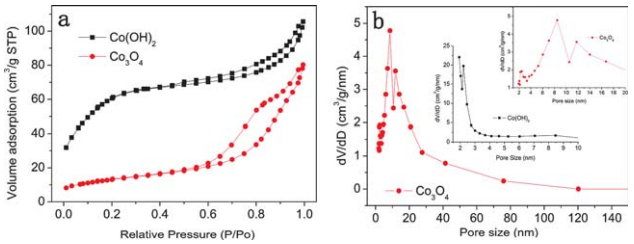

Fig. 4 (a) Nitrogen adsorption/desorption isotherms curves at 77 K of the triangle taper-like microcrystals; (b) pore size distribution curve of Co_3O_4 after calcined at 400 °C for 4 h; inset is the enlarged pore size distribution curve of Co_3O_4 and the pore size distribution curve of $Co(OH)_2$.

9.1 nm, which coincided well with the HRTEM image. The BJH adsorption cumulative pore volume is 0.122 and 0.126 $cm^3\ g^{-1}$ for $Co(OH)_2$ and Co_3O_4 sample, respectively. It is expected that such mesoporous structure will provide better contact for the electrolyte and channels for ion diffusion.

2. Formation of cobalt hydroxide

In order to investigate the formation mechanism of the triangle taper-like β-$Co(OH)_2$ microsrystals, detailed time-dependent experiments were carried out at 95–100 °C. From the TEM and SEM images of these products shown in Fig. 5 and 6, the morphology evolution of the structure is observed clearly. When the reaction time was several minutes (Fig. 5a), a bowtie-like nanocolumns with scale about 200 nm to 400 nm formed. With the reaction time increased to 60 min (Fig. 5b and Fig. 6a), the bowtie-like columns grew up, the diameter increased to 0.5–0.8 μm and length increased to 1.5–2.0 μm. After 90 min, columns with a smoother surface and the length from 2.0 μm to 3.0 μm are obtained. This crystal growth followed the typical

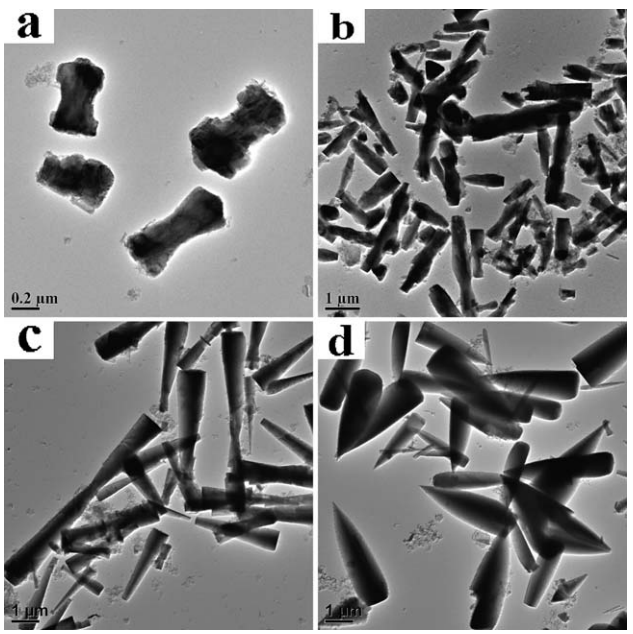

Fig. 5 TEM images of $Co(OH)_2$ samples synthesized at different time (a) several minutes, (b) 60 min; (c) 105 min and 120 min.

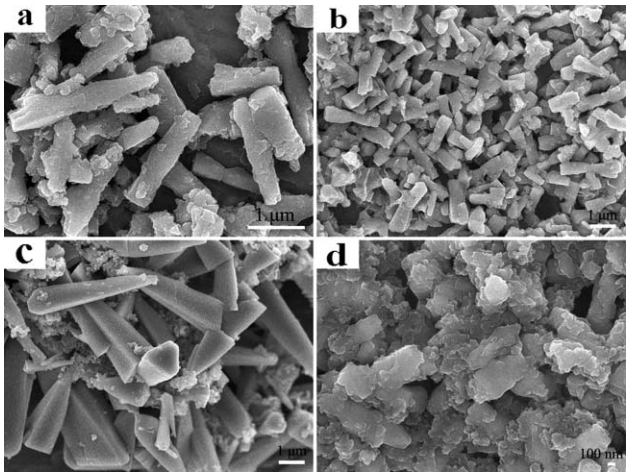

Fig. 6 SEM images of $Co(OH)_2$ samples synthesized at different time (a) 60 min, (b) 90, (c) 180 and (d) 240 min.

Ostwald ripening process. When the reaction time was prolonged to 105 min (Fig. 5c), some triangle taper-like structures with length from 2.5–4.0 μm formed and small nanoparticles are observed. After 120 min, a taper-like structure with equilateral triangle at the tip and end are observed (Fig. 2c and inset). This process was controlled by a possible dissolve-reconstruction approach.[28] The triangle taper-like structure with length from 4.0–5.0 μm are formed when the reaction time prolonged to 180 min (Fig. 6c). The triangle taper structure was destroyed after 240 min (Fig. 6d), columns with rough surface and lots of nanoparticles are observed. The XRD curves of the $Co(OH)_2$ prepared at different times are shown in Fig. S1 (ESI†). All the diffraction peaks are well indexed to pure hexagonal phase of β-$Co(OH)_2$ according to JCPDS 30-0443. On the basis of experimental results, a possible formation mechanism in the growth process is shown in Fig. 7.

When the reaction time was less than 90 min, the typical Ostwald ripening process played the dominated role in the crystal growth. After 90 min, the dissolve-reconstruction approach in basic condition took over, and the two steps produced the triangle taper-like structures. According to these results, the chemical reactions occurred can be expressed as:

$$Co^{2+} + 2NH_4OH \rightleftharpoons Co(OH)_2(s) + 2NH^+_4 \quad (1)$$

$$Co(OH)_2(s) + NH_4OH \rightleftharpoons HCoO^-_2 + NH^+_4 + H_2O \quad (2)$$

$$Co(OH)_2(s) \rightleftharpoons HCoO^-_2 + H^+ \quad (3)$$

$$Co(OH)_2(aq) \rightleftharpoons H^+ + HCoO^-_2 \quad (4)$$

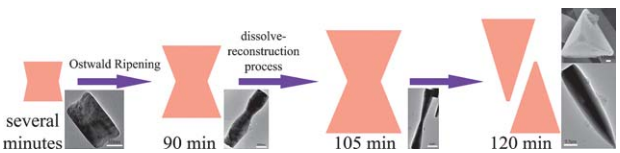

Fig. 7 Schematic illustration of the formation mechanism of triangle taper-like $Co(OH)_2$ structure.

Following the reactions (1) to (4), the finally dissolve-reconstruction approach follows the reaction:

$$Co(OH)_2(s) \rightleftharpoons Co(OH)_2(aq) \quad (5)$$

3. Electrochemical study

The electrochemical properties of the mesoporous β-$Co(OH)_2$ and Co_3O_4 samples were investigated by cyclic voltammetry (CV). Fig. 8 show the CV curves with different scan rates of the two samples. As shown in Fig. 8a, the peak P2 is due to the oxidation of Co(II) to Co(III) and the P4 corresponded to the reverse process; the anodic peak P1 is due to the oxidation of Co(III) to Co(IV) and the P3 is for the reverse process.[29] Fig. 8b is the CV curves of the mesoporous Co_3O_4 microcrystals at different scan rates, two pairs of redox peaks are visible in the CV curves. All the capacitive characteristics are different from the electric double-layer capacitance. It shows that the capacitance mainly results from a pseudo-capacitive capacitance caused by reversible electrochemical reaction. The specific capacitance values are calculated based on the CV results according to the equation shown in ref. 30. The specific capacitances are 137.6, 124.8, 108.8 and 98.0 F g^{-1} at scan rates of 5, 10, 20 and 50 mVs^{-1} for β-$Co(OH)_2$; 91.5, 97.4, 90.7 and 70.9 F g^{-1} for Co_3O_4 sample at scan rates of 5, 10, 20 and 50 mVs^{-1}, which are similar to the results reported before.[19] Co_3O_4 microcrystals might have potential application as electrode materials for supercapacitors.

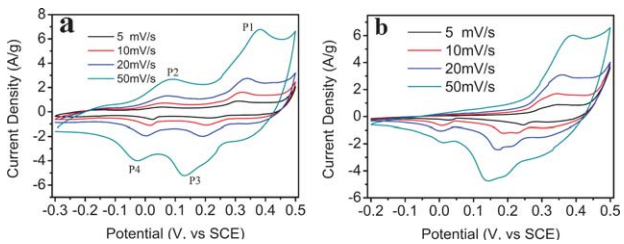

Fig. 8 Cyclic voltammetry curves at different scan rates (a) $Co(OH)_2$, (b) Co_3O_4.

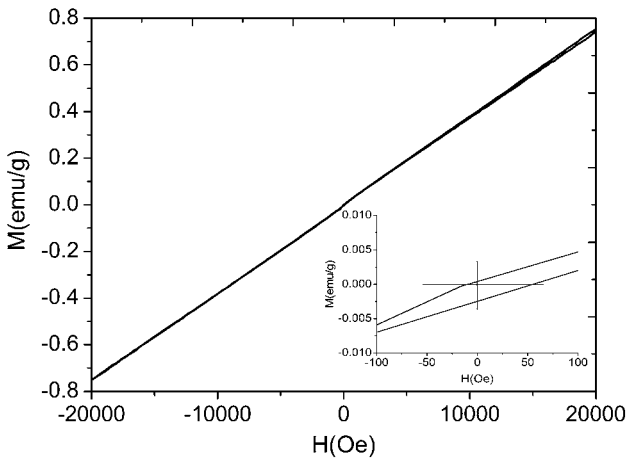

Fig. 9 Hysteresis loops of the triangle taper-like Co_3O_4 at room temperature. The inset is the magnified *M-H* hysteresis loop.

4. Magnetic study

The magnetic properties of the sample have been investigated (Fig. 9). The shape of the magnetic curve is very similar to Co_3O_4 porous nanotubes,[31] nanowires[32] and the previous study by our group.[11] The curves show a small ferromagnetic component, as a little low coercive force and remnant magnetization can be seen. The larger surface area of the Co_3O_4 (a BET surface area of 47 m^2 g^{-1}) increases the uncompensated spins of surface, that leads to an increase of the coercive force and the horizontal shift of the hysteresis loop. With applied field of 2 T, the magnetization is about 0.75 emu/g at room temperature.

Conclusions

In summary, the triangle taper-like β-$Co(OH)_2$ and mesoporous Co_3O_4 microcrystals have been synthesized *via* a simple solid state crystal reconstruction approach and an Ostwald ripening and dissolve-reconstruction approach have been discussed. The specific capacitances are 91.5, 97.4, 90.7 and 70.9 F g^{-1} for Co_3O_4 sample at scan rates of 5, 10, 20 and 50 mV s^{-1}, these showed an improved electrochemical performance as electrode materials for supercapacitors. With applied field of 2 T, the magnetization is about 0.75 emu g^{-1} of the triangle taper-like Co_3O_4 at room temperature. The as-prepared mesoporous Co_3O_4 nanostructures are expected to have great applications in many fields.

Acknowledgements

This work is supported by the National Nature Science Foundation of China (No. 50972153), the Shanghai Nanotechnology Promotion Center (0852nm01900) and Shanghai Talents Program Foundation.

Notes and references

1 P. G. Bruce, B. Scrosati and J. M. Tarascon, *Angew. Chem., Int. Ed.*, 2008, **47**, 2930–2946.
2 X. W. Lou, Y. Wang, C. L. Yuan, J. Y. Lee and L. A. Archer, *Adv. Mater.*, 2006, **18**, 2325.
3 M. Long, W. M. Cai, J. Cai, B. X. Zhou, X. Y. Chai and Y. H. Wu, *J. Phys. Chem. B*, 2006, **110**, 20211–20216.
4 C. Y. Lai, B. G. Trewyn, D. M. Jeftinija, K. Jeftinija, S. Xu, S. Jeftinija and V. S. Y. Lin, *J. Am. Chem. Soc.*, 2003, **125**, 4451–4459.
5 G. Binotto, D. Larcher, A. S. Prakash, R. H. Urbina, M. S. Hegde and J. M. Tarascon, *Chem. Mater.*, 2007, **19**, 3032–3040.
6 C. Largeot, C. Portet, J. Chmiola, P. L. Taberna, Y. Gogotsi and P. Simon, *J. Am. Chem. Soc.*, 2008, **130**, 2730.
7 J. Feng and H. C. Zeng, *J. Phys. Chem. B*, 2005, **109**, 17113–17119.
8 R. Xu and H. C. Zeng, *Langmuir*, 2004, **20**, 9780–9790.
9 H. Zhang, J. B. Wu, C. X. Zhai, X. Y. Ma, N. Du, J. P. Tu and D. R. Yang, *Nanotechnology*, 2008, 19.
10 R. Xu and H. C. Zeng, *J. Phys. Chem. B*, 2003, **107**, 12643–12649.
11 Y. Z. Shao, J. Sun and L. Gao, *J. Phys. Chem. C*, 2009, **113**, 6566–6572.
12 K. T. Nam, D. W. Kim, P. J. Yoo, C. Y. Chiang, N. Meethong, P. T. Hammond, Y. M. Chiang and A. M. Belcher, *Science*, 2006, **312**, 885–888.
13 X. W. Lou, D. Deng, J. Y. Lee, J. Feng and L. A. Archer, *Adv. Mater.*, 2008, **20**, 258.
14 X. W. Xie, Y. Li, Z. Q. Liu, M. Haruta and W. J. Shen, *Nature*, 2009, **458**, 746–749.
15 B. Z. Tian, X. Y. Liu, H. F. Yang, S. H. Xie, C. Z. Yu, B. Tu and D. Y. Zhao, *Adv. Mater.*, 2003, **15**, 1370.
16 W. B. Yue, A. H. Hill, A. Harrison and W. Z. Zhou, *Chem. Commun.*, 2007, 2518–2520.
17 W. B. Yue and W. Z. Zhou, *J. Mater. Chem.*, 2007, **17**, 4947–4952.

18 Y. G. Li, B. Tan and Y. Y. Wu, *J. Am. Chem. Soc.*, 2006, **128**, 14258–14259.
19 Y. G. Li, B. Tan and Y. Y. Wu, *Nano Lett.*, 2008, **8**, 265–270.
20 X. W. Lou, D. Deng, J. Y. Lee and L. A. Archer, *J. Mater. Chem.*, 2008, **18**, 4397–4401.
21 F. M. Zhan, B. Y. Geng and Y. J. Guo, *Chem.–Eur. J.*, 2009, **15**, 6169–6174.
22 S. L. Xiong, C. Z. Yuan, M. F. Zhang, B. J. Xi and Y. T. Qian, *Chem.–Eur. J.*, 2009, **15**, 5320–5326.
23 G. X. Wang, X. P. Shen, J. Horvat, B. Wang, H. Liu, D. Wexler and J. Yao, *J. Phys. Chem. C*, 2009, **113**, 4357–4361.
24 W. J. Zhou, M. W. Xu, D. D. Zhao, C. L. Xu and L. Li, *Microporous Mesoporous Mater.*, 2009, **117**, 55–60.
25 F. F. Tao, C. L. Gao, Z. H. Wen, Q. Wang, J. H. Li and Z. Xu, *J. Solid State Chem.*, 2009, **182**, 1055–1060.
26 Y. Liu, W. W. Zhao and X. G. Zhang, *Electrochim. Acta*, 2008, **53**, 3296–3304.
27 Y. Shan and L. Gao, *Chem. Lett.*, 2004, **33**, 1560–1561.
28 K. H. Gayer and A. B. Garrett, *J. Am. Chem. Soc.*, 1950, **72**, 3921–3923.
29 L. B. Kong, J. W. Lang, M. Liu, Y. C. Luo and L. Kang, *J. Power Sources*, 2009, **194**, 1194–1201.
30 X. F. Xie and L. Gao, *Carbon*, 2007, **45**, 2365–2373.
31 R. M. Wang, C. M. Liu, H. Z. Zhang, C. P. Chen, L. Guo, H. B. Xu and S. H. Yang, *Appl. Phys. Lett.*, 2004, **85**, 2080–2082.
32 Z. Dong, Y. Y. Fu, Q. Han, Y. Y. Xu and H. Zhang, *J. Phys. Chem. C*, 2007, **111**, 18475–18478.

